J. Fluid Mech. (1984), *vol.* 149, *pp.* 319–337
Printed in Great Britain

The structure of a turbulent spot in Blasius flow

By J. BARROW, F. H. BARNES, M. A. S. ROSS
Physics Department, University of Edinburgh
AND S. T. HAYES
Edinburgh Regional Computer Centre

(Received 14 February 1983 and in revised form 9 July 1984)

Turbulent spots formed artificially in a Blasius boundary layer have been investigated over a finite width extending across the plane of symmetry of the spots. Hot wires were used to measure the local mean and fluctuating parts of the downstream and spanwise velocity components, and the third component was computed. The results are presented in contour diagrams, and are compared with previous published work.

The values of energy thickness in the spots are computed from the contours of downstream velocity. The spots are found to consist of an upper part containing most of the turbulence, moving over a lower layer whose contribution to the energy thickness is small. When, near the rear of the spot, the energy thickness decreases to the value in Blasius flow, the two parts recombine, and the flow slowly regains the Blasius velocity profile.

The spots grow by entrainment of laminar fluid, and the physical principles governing this process are discussed.

1. Introduction

The main facts about turbulent spots in Blasius flow were known by 1960. Emmons (1951) reported their spontaneous occurrence and their aggregation to form turbulent boundary layers. Schubauer & Klebanoff (1956), using hot wires to detect turbulence, observed their apparently invariant shape in plan and elevation, and their rates of propagation and growth. Elder (1960) obtained the first photographs, and these showed much turbulence, a very rough front, and trailing vortices. Further work was clearly needed to understand the mechanics of the spots, but such work called for fast methods of velocity measurement which did not become available for another ten years. In the meantime, the idea gained favour that a single coherent vortex might be responsible for the form of the spots. It was also generally assumed that the symmetry of the spots in plan implied zero mean spanwise flow on the centreplane, $z = 0$.

Wygnanski, Sokolov & Friedman (1976) (WSF) used a wind tunnel with a vertical flat plate to make hot-wire measurements of the velocity components U (downstream), V (normal) and W (spanwise) at a range of x-stations and of (y, z) positions within spots. Each recording was digitized at 10^4 s^{-1} per channel. To improve the discrimination between laminar and turbulent flow, the spectrum of each recording was limited to 40–1600 Hz, and further smoothing was used. The times of arrival of the leading and trailing edges (LE and TE) of turbulence were found, and, in repeated recordings, small variations occurred in the interval TE–LE. Ensemble averages of such recordings were found by matching LE or TE times. The authors encountered problems with both the general level of the very small V-component, and the non-zero

value of W observed at $z = 0$; these were attributed to errors of measurement. The spots were found to grow in height at about the same rate as a turbulent boundary layer. Since calculated streamlines depend on the assumed mean velocity of propagation, double correlation coefficients of U on the centreplane were computed. An eddy moving downstream at $0.65U_0$ was located near the plate and near the front of the spot. A streamline diagram obtained with this velocity was then presented as a function of normalized time.

Following preliminary work by Coles & Barker (1975) on turbulent spots formed in a water channel, Cantwell, Coles & Dimotakis (1978) (CCD) made measurements of $U(t)$ on the centreplane of spots, using a laser-Doppler method. Their results are similar to ours. Three x-positions were used. $U(t)$ at constant x was transformed to $U(x)$ at constant t by conical projection, and the velocity potential was derived from $U(x)$. The Bernoulli equation for unsteady flow was then used to compute C_p at the plate. (Direct measurements of C_p at the plate by Mautner & Van Atta (1982) (MA) are now available.) Then, assuming $W = 0$ at $z = 0$, the stream function $\psi(x, y, t)$ was computed in two stages from the original data. ψ in laboratory coordinates was transformed to a system with moving axes, first with x-axis speed $0.78U_0$, and then with the addition of a y-axis speed of $0.0037U_0$. The resulting streamlines and particle paths indicated two eddies within the spot. Finally, estimates of entrainment were computed for the different parts of the outline of the spot in the centreplane.

Following preliminary work by Van Atta & Helland (1980), Antonia *et al.* (1981) (ACSA) used a wind tunnel and a horizontal flat plate, the surface of the plate being held at $\Delta T = 10$ °C above air temperature. Measurements of U, V and T were made on the centreplane of the spots. Recordings were digitized at 3200 s^{-1} per channel, and ensemble averages were obtained by matching leading edges of the turbulence. Averages of 200 runs gave mean values of U, V and T. Single runs gave deviations from the means, u, v and θ, and mean values for all quadratic products of deviations such as $\langle u^2\rangle^{\frac{1}{2}}$ and $\langle uv\rangle$. Differences between the measured properties and those in Blasius flow were expressed non-dimensionally. The graphs of $(\bar{U} - U_B)/U_0$ are not complete close to the plate. They found

(i) at the two lowest y-positions $-\langle uv\rangle$ rises abruptly at the front of the spot, and falls abruptly after 2 or 3 ms, indicating a short region of high turbulence;

(ii) at the same y-positions $\langle u^2\rangle^{\frac{1}{2}}$ and $\langle v^2\rangle^{\frac{1}{2}}$ rise abruptly to a definite peak and fall quite slowly;

(iii) $(\bar{V} - V_B)/U_0$ is negative at the lowest level; the normal velocity near the plate must therefore consist almost entirely of low-turbulence fluctuations.

Wygnaski, Haritonidis & Kaplan (1979) (WHK) used 'rakes' of parallel hot wires, assembled for y- or z-surveys of the flow. The original purpose of the work was to search for evidence of coherent vortex structures in the spots or in the laminar flow just outside the turbulent region. No such evidence was found, but wave packets of Tollmien–Schlichting type were found upstream of the wings of the spots. The paper by Wyganski, Zilberman and Haritonidis (1982) (WZH) is useful insofar as it shows the limitations of a geometrical approach to the problems of turbulent spots in Blasius flow (including their entrainment). New measurements of U and V were made on the centreplane of the spots, and used to examine growth rates in x, y and (using results from other work) in z. It is concluded that the spots are not self-similar in 3 dimensions. The authors find that a $+30\,\%$ correction is necessary in the positive maximum values of $(U - U_B)/U_0$ taken from earlier ensemble-averaged results.

The results that form the substance of the present paper were obtained many years ago, in a limited time before the wind tunnel was dismantled for removal to another

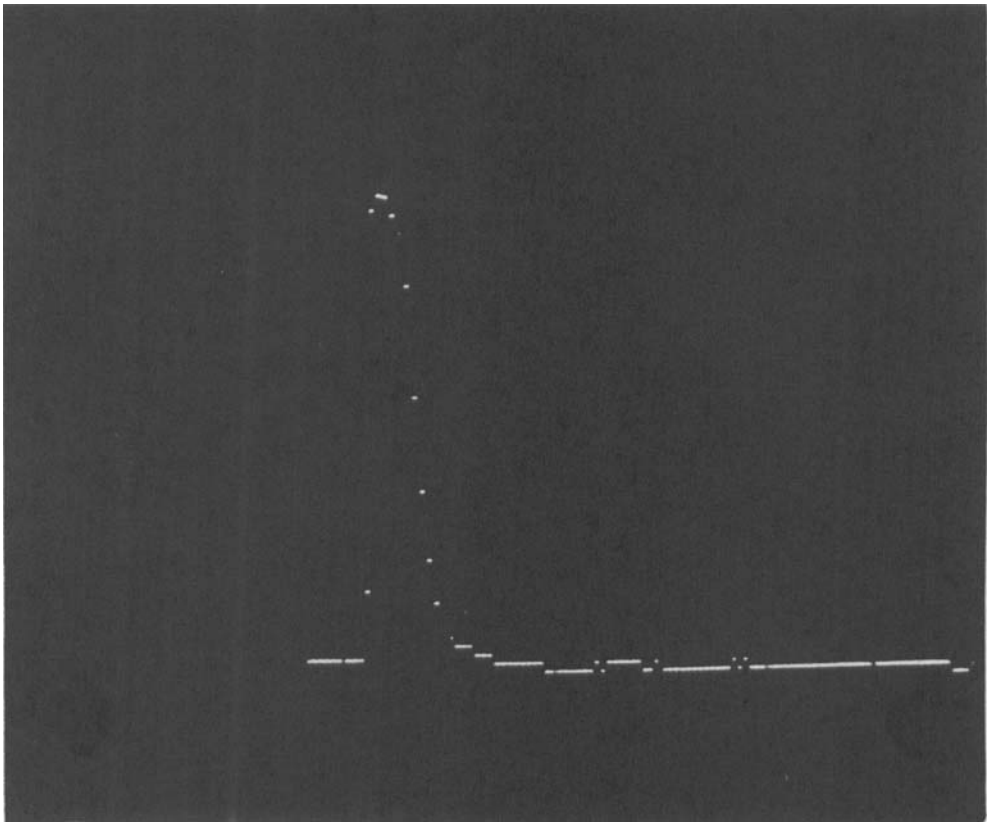

FIGURE 1. Oscilloscope display of hot-wire measurements of the velocity in the air jet recorded at 8 kHz, with no flow in the wind tunnel.

building. When reduction of data and preparation of contour diagrams was completed, the results were in some respects unexpected, and the work was given only limited publication by Barrow (1975). The records have been reexamined recently, and are thought to be useful in providing a clear mental image of various details within the spots. Calculations of energy thickness in the spot have been introduced.

2. Experimental equipment and procedure

The work was done in the 4 ft × 4 ft (1.22 m × 1.22 m) low-turbulence wind tunnel designed for boundary-layer studies. The free-stream speed U_0 was continuously monitored and regulated by the method of Robertson & Burns (1972) to maintain U_0 constant to $\pm 0.1\,\%$. A perspex flat plate with a machined leading edge was mounted in the central vertical plane of the working section. The pressure gradient $(\mathrm{d}p/\mathrm{d}x)/\frac{1}{2}\rho\, U_0^2$ did not exceed 0.1 % per foot, and the total ambient turbulence level above 8 Hz did not exceed 0.035 % at speeds up to 45 ft/s (14 m/s). Turbulent spots were produced by injection into the boundary layer of a 1.5 ms pulse of air of constant volume, through a 1 mm diameter hole on the centreline of the plate at 1 ft from the leading edge (figure 1). The probe carried two hot wires lying parallel to the plate and close to each other, one sensitive to U and the other to U and W.

During the passage of a turbulent spot over the probe, the voltage on each hot wire was digitized 128 times at a rate for each wire of 1500 s^{-1} – about $\frac{1}{2}$ the rate used by

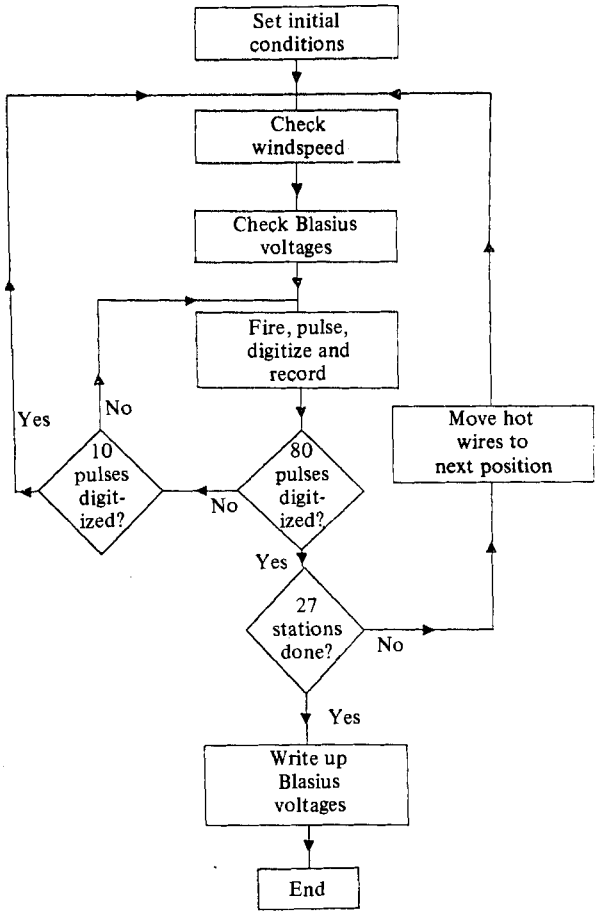

FIGURE 2. Flow diagram of the program for computer operation of a single run.

ACSA. Readings were recorded as 12 bit words on magnetic tape. The time delay between spot excitation and the start of recording was a two-loop computer delay giving adjustment in units of 0.25 ms.

An experiment at given U_0 and x-position of the probe consisted of 6 runs at intervals $\Delta z = 0.5$ in (1.27 cm) spanning the centreline of the plate. Each run recorded 80 spots at each of 27 y-positions, starting close to the plate. y-positions were set by the computer, and typical values of Δy were 0.03δ for the lowest 10 settings, 0.09δ for the next 9, and 0.18δ for the last 8, where δ is the total thickness of the Blasius layer to $0.99U_0$. A flow diagram of the computer program for a run is shown in figure 2. The Blasius profile was read at 18 positions, providing a check on the initial y-position and on the sensitivity of the hot wires. Time is measured by t in seconds from the time of spot excitation, and by T in units of 1500^{-1} s from the start of recording.

The voltage readings were analysed to give mean values $\overline{U}$, $\overline{W}$ and standard deviations u', w' and the induced velocity $\overline{U} - U_B$, all expressed relative to U_0. The averages were taken at constant T.

To obtain contour diagrams of any one of the four measured variables represented now by X, it was convenient to have values of X at equal intervals of t, y and z. Values of X at constant $\Delta y = 0.05\delta$ were therefore found using 3 terms of Newton's

	U_0		Probe position		
Experiment	(ft/s)	(m/s)	x (ft)	x (m)	R
1	28.5	8.69	2.427	0.740	1147
2	28.5	8.69	3.430	1.045	1364
3	43.5	13.26	3.427	1.045	1685
4	43.5	13.26	3.925	1.196	1805
5	43.5	13.26	4.420	1.347	1912

TABLE 1. Details of the five main experiments

interpolation formula for unequal intervals. A least-squares method was then developed by one of the authors (STH) to invert the function $X = f(t, y, z)$ to relations such as $y = F(X, t, z)$ for given z and fixed increments in X. The gradients $\partial\overline{U}/\partial t$ and $\partial\overline{W}/\partial z$ were found, and it was assumed that

$$\frac{\partial\overline{V}}{\partial y} = -\frac{1}{U_a}\frac{\partial\overline{U}}{\partial t} - \frac{\partial\overline{W}}{\partial z},$$

where U_a is the mean rate of advance of the fluid. Then to a good approximation $\overline{V}(y)$ is given by

$$\int_0^y \frac{\partial\overline{V}}{\partial y}\,\mathrm{d}y.$$

The velocity measurements are available in the archives of EMAS (Edinburgh Multi Access System).

3. Experimental results

Table 1 shows details of the five main experiments. The 6 runs in each experiment are identified by the letters (*a*)–(*f*) in order of decreasing z-position. Since the searched cross-section of the spots was limited in z to 2.5 in. (6.4 cm), and in y to 2.5δ, experiment 1 shows most of the crest and wings, while experiment 5 shows in greater detail the lower part of the spot around the centreplane.

Figures 3, 4 and 5 show contour diagrams of $\overline{U}/U_0$, u'/U_0 and $\overline{V}/U_0$ for experiment 1, where the centreplane lies slightly above run (*d*).† The contour intervals are 5 % in figure 3 and 2 % in figure 4. In figure 5, contours for runs (*a*), (*c*) and (*d*) are shown at 1 % intervals with the zero contour omitted; continuous lines have positive values and dashed lines negative ones. Figure 6 shows contour diagrams for run (*b*) of experiment 5, where run (*c*) coincides with the centreplane. Figure 6(i) shows $(\overline{U} - U_B)/U_0$ at 5 % intervals; the dashed line is the zero contour, with positive contours below it and negative above. Figure 6(ii) shows contours of $-\overline{W}/U_0$ from $y = 0$ to $y = 0.5\delta$ at 4 % intervals with the zero contours indicated.

Figure 3 shows the following features. (i) In run (*d*) there is an early first deflection of the $0.95U_0$ contour where the true nose should be seen, a smaller deflection begins at a lower level in run (*c*), but in other runs the first deflections develop gradually, forming a roughly parabolic front below the nose. (ii) Although there is a difference of 30 T-units between first deflections of contours in runs (*d*) and (*a*), the crest in all 6 runs arrives within a few T-units of $T = 40$. Spanwise convection may be significant there.

† Estimates of errors of measurement affecting figures 3 and 4 are discussed in the Appendix.

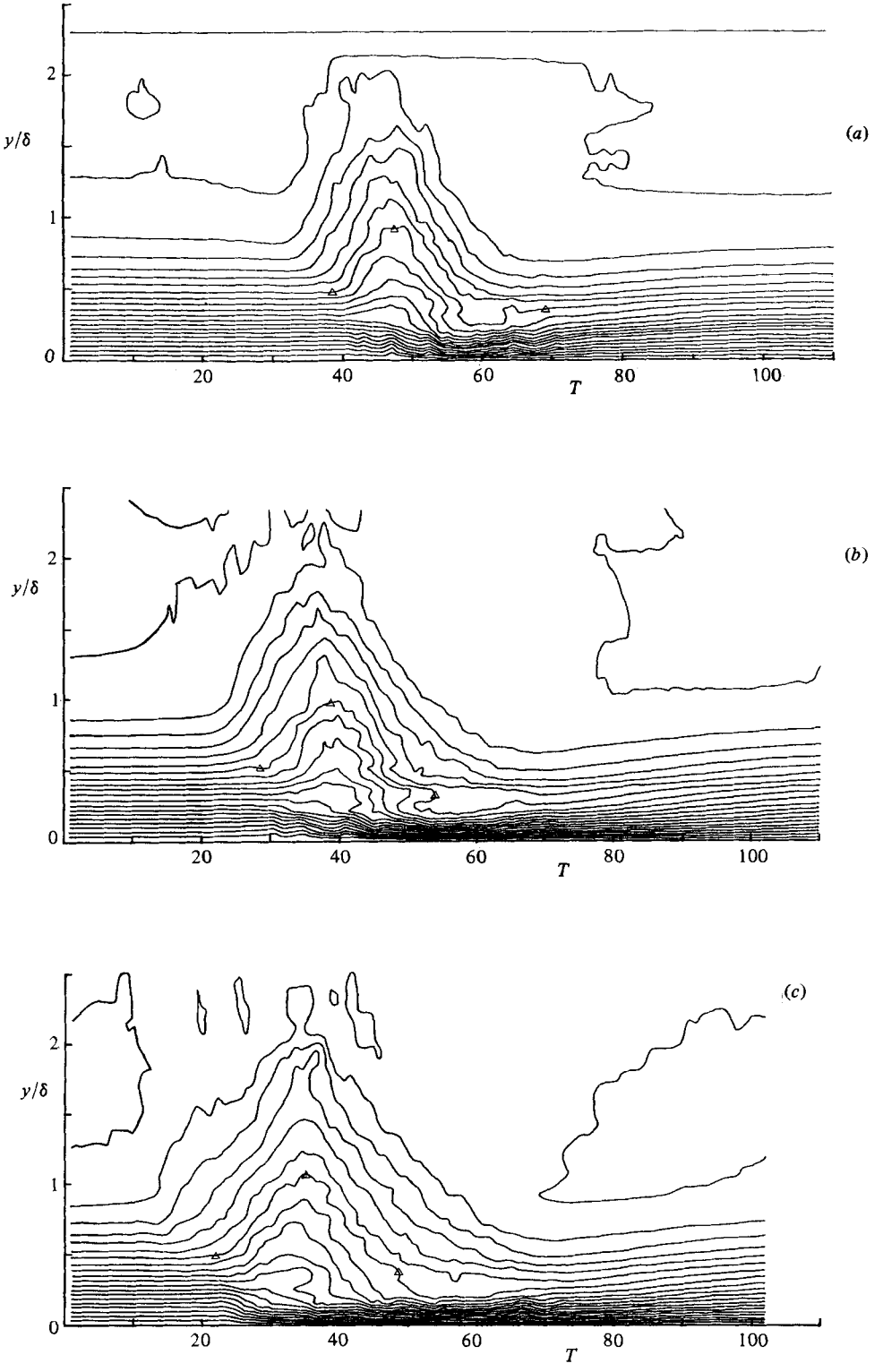

FIGURE 3(*a*, *b*, *c*). For caption see facing page.

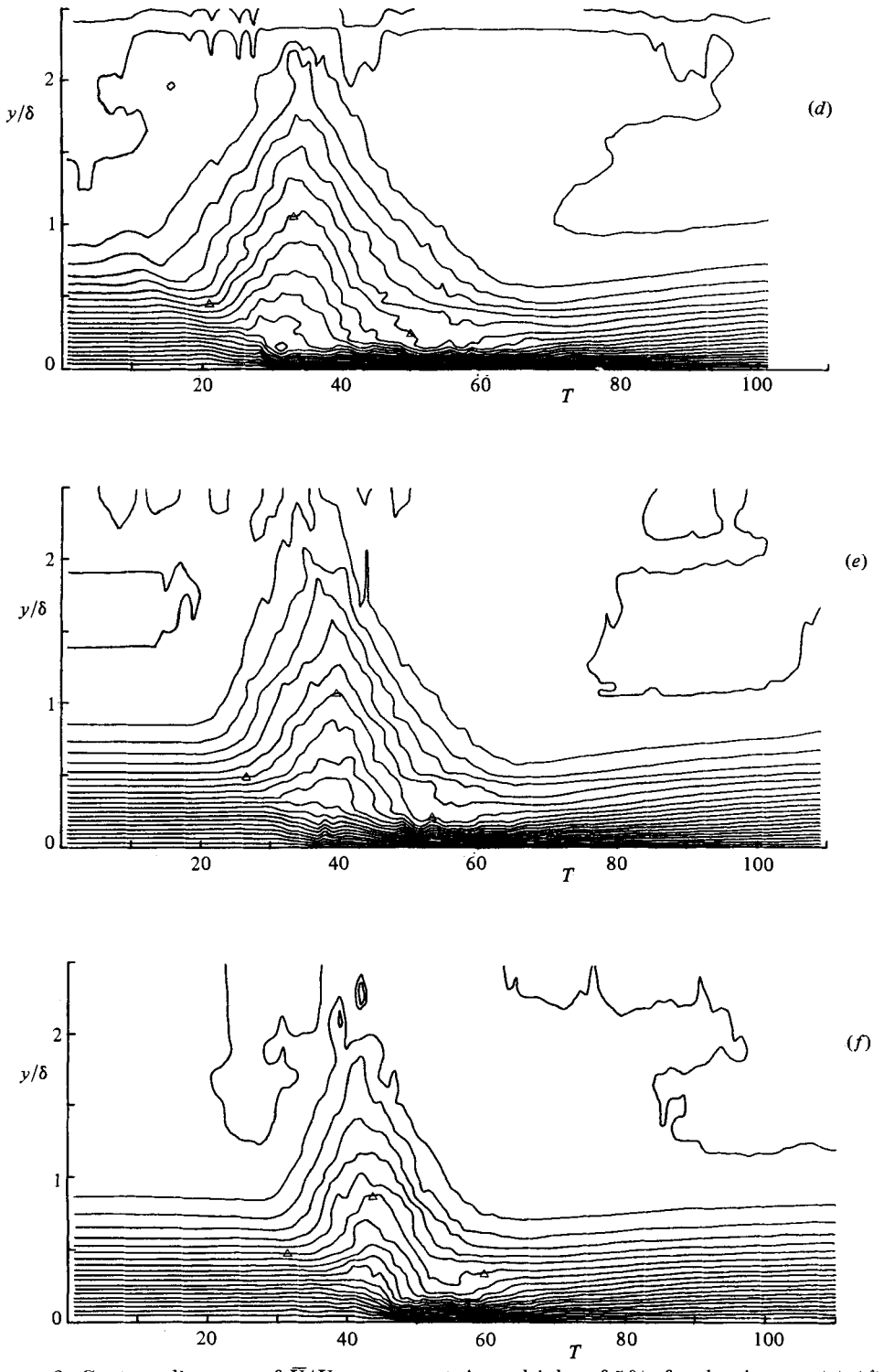

FIGURE 3. Contour diagrams of $\bar{U}/U_0$ = constant, in multiples of 5%, for the six runs (*a*)–(*f*) of experiment 1. $U_0 = 28.5$ ft/s (8.69 m/s), $x = 2.427$ ft (74 cm). Contours for $\bar{U}/U_0 = 0.70$ are marked with open triangles.

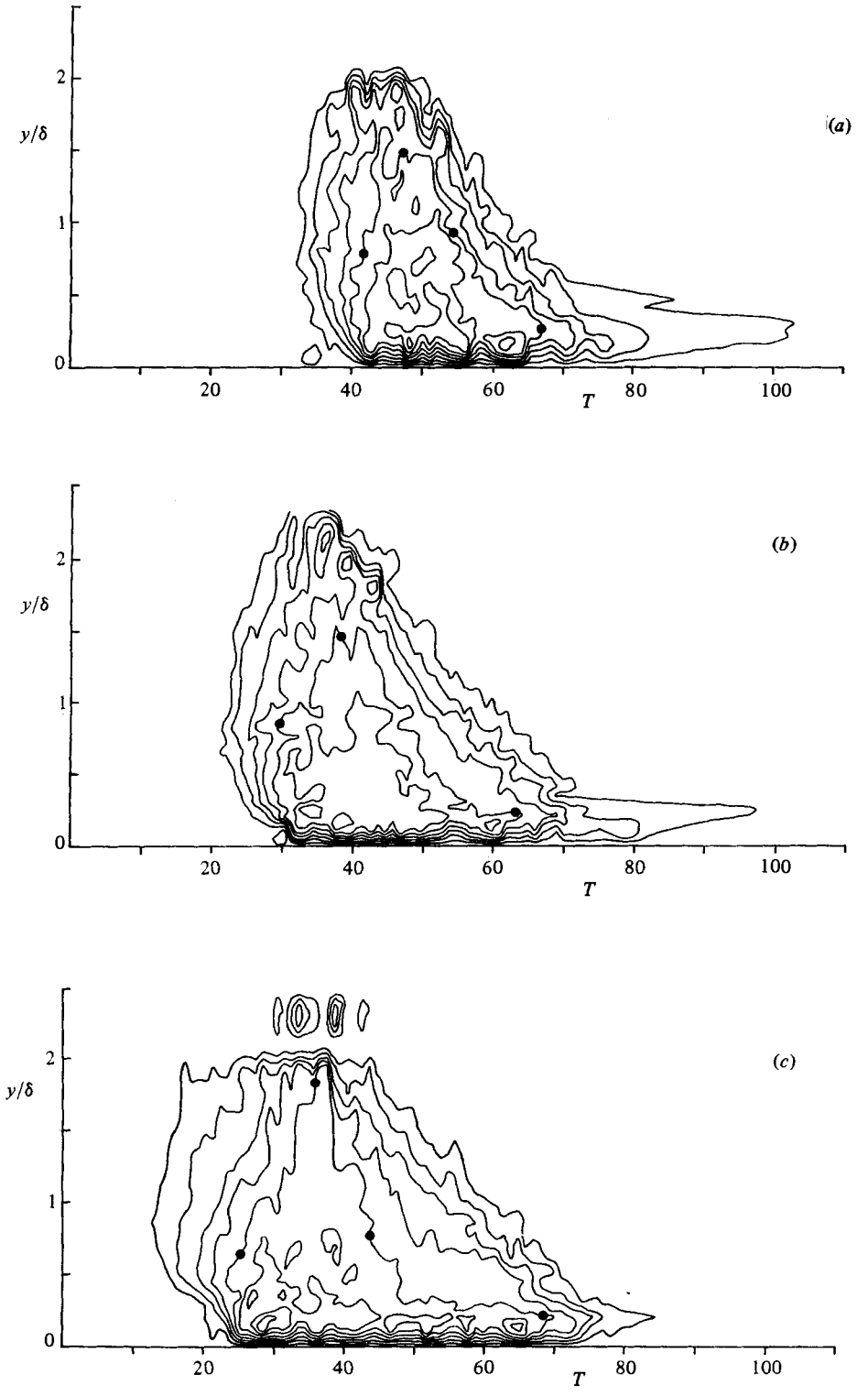

FIGURE 4(*a*, *b*, *c*). For caption see facing page.

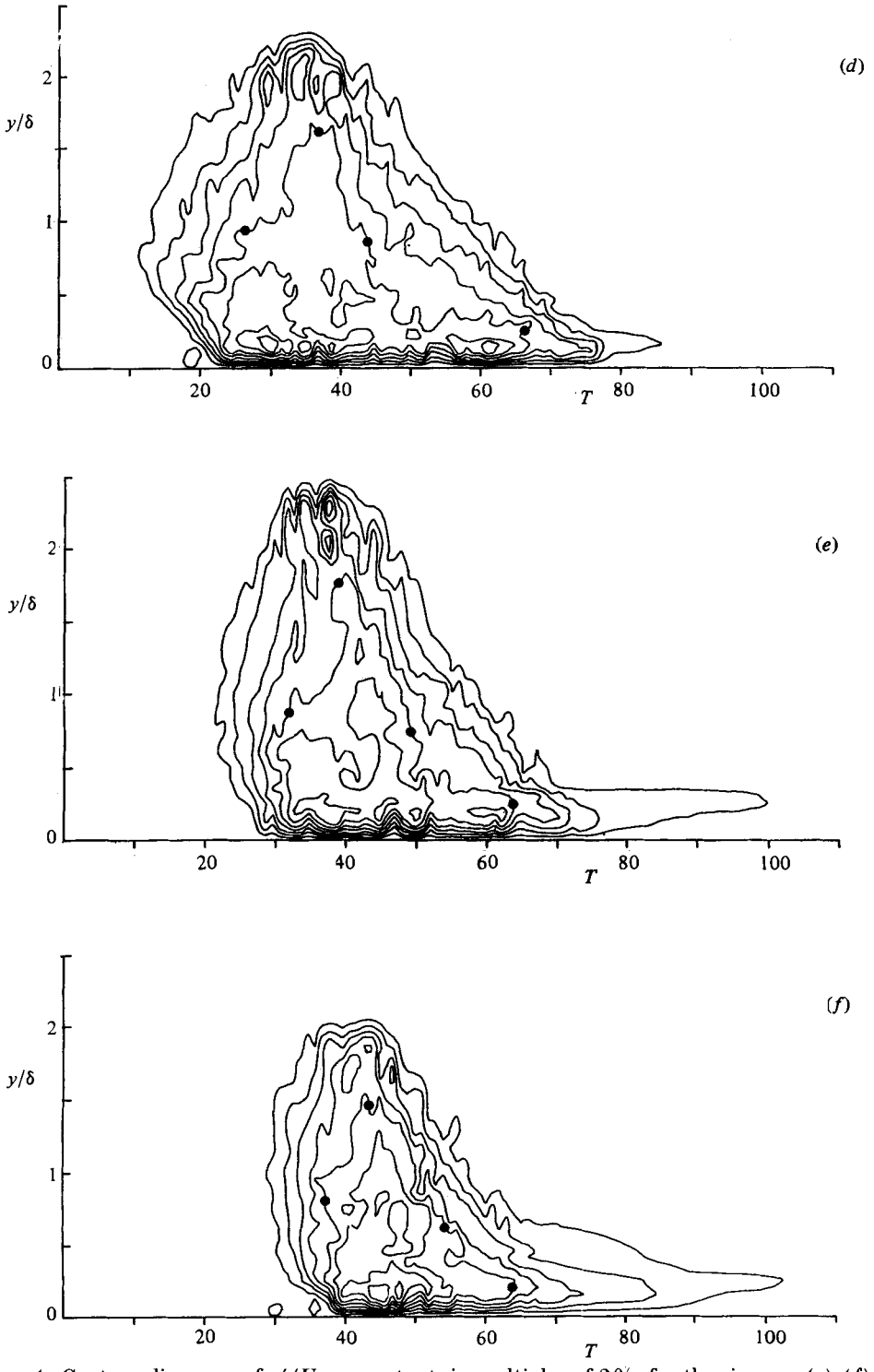

FIGURE 4. Contour diagrams of u'/U_0 = constant, in multiples of 2%, for the six runs (*a*)–(*f*) of experiment 1. $U_0 = 28.5$ ft/s (8.69 m/s), $x = 2.427$ ft (74 cm). Contours for $u'/U_0 = 10\%$ are marked with solid circles.

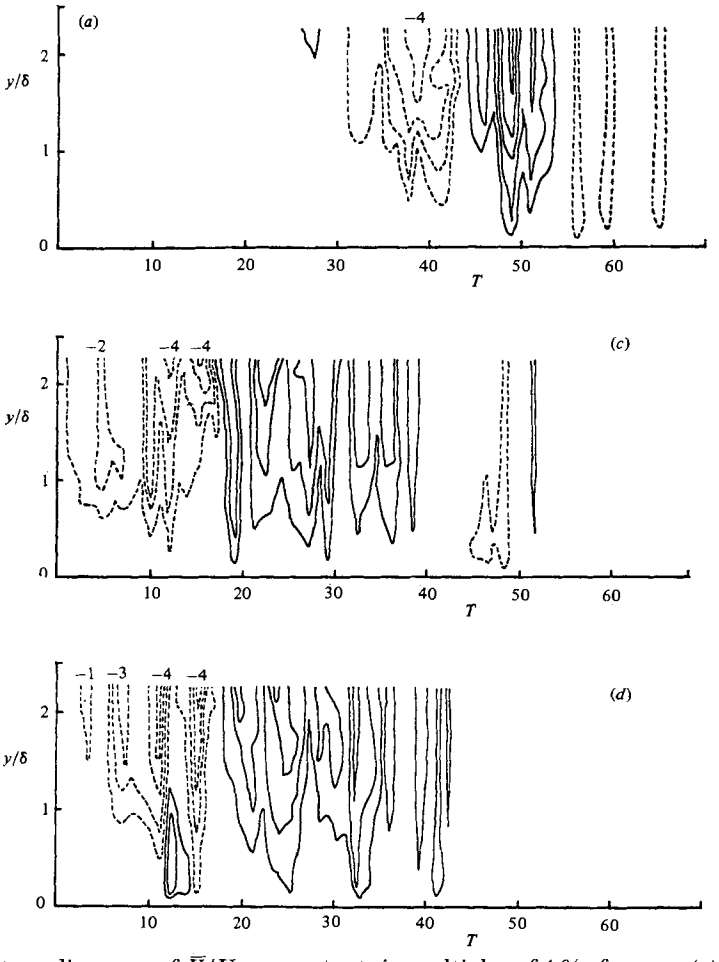

FIGURE 5. Contour diagrams of $\overline{V}/U_0$ = constant, in multiples of 1 %, for runs (*a*), (*c*) and (*d*) of experiment 1. $U_0 = 28.5$ ft/s (8.69 m/s), $x = 2.427$ ft (74 cm). Zero contour omitted. ——, positive contours; – – – –, negative contours. The strength % of negative pulses is shown above the figures.

Close to the plate $\partial\overline{U}/\partial y$ has high values, highest on the centreplane. Figure 6(i), which closely resembles figure 12 (after WSF) in Zilberman, Wygnanski & Kaplan (1977), shows more details of the flow. Moving forward from the rear of the spot, at $y \approx 0.12\delta$ (where $U_B \approx 0.2U_0$), $\overline{U} - U_B$ reaches $+0.45U_0$ at $T = 100$, and falls slowly to $+0.25U_0$ at $T = 30$. In experiments 1–4 the corresponding contours are $+0.40U_0$ and $+0.20U_0$.

The next contour that must be taken seriously is the zero contour of $\overline{U} - U_B$, which lies ahead of the turbulence front, and indicates some disturbance of the Blasius flow by downstream, normal and possibly spanwise velocity components. Between the 25 % and zero contours there lies the turbulence front, which is known to be propagated at $\sim 0.88U_0$. A high value of $\overline{U}$ is not recorded there, and it must be inferred that high turbulence production is the main reason for the high rate of advance of the front. The measurements of C_p in this region by MA show, moving forwards through this front, first a steep rise, followed by a steep fall to a slight dip, and this confirms the idea that turbulence production is strongest at the actual front.

Figure 4 provides evidence of the turbulence. (i) The survival of the large eddies

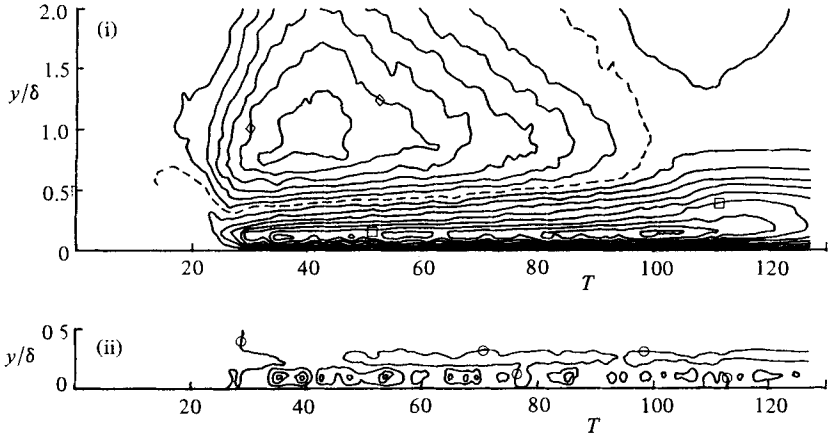

FIGURE 6. (i) Contour diagram of $(\bar{U}-U_B)/U_0$ = constant in 5% intervals for run (*b*) of experiment 5. $U_0 = 43.5$ ft/s (13.26 m/s), $x = 4.420$ ft (1.347 m). ----, zero contour; ——, non-zero contours; positive below and negative above the zero contour. ◇, −25%; □, +30%. (ii) Contour diagram of $-\bar{W}/U_0$ = constant in 4% intervals, in the sublayer of run (*b*) in experiment 5. The zero contours are marked with open circles.

at the crest in averaged results implies some regularity in the production of eddies, which occur at intervals of about $5T$. (ii) The only evidence of a 'turbulence nose' is a small blunt projection in figure 4(*d*) at $T = 11$ and $y = 0.86\delta$. Both above and below this projection, the front contours in this run slope quite strongly towards the rear of the spot. As $|z|$ increases, however, the front becomes only slightly convex, and nearly parallel to the y-axis. (iii) The observed values of u'/U_0 rise to at least 16%. The highest values occur near the front of the spot and elsewhere at y-levels between 0.12 and 0.25δ. These observations are consistent with those in figure 11(*g*) of ACSA, who found a Reynolds-stress peak near the front of the spot in recordings at $y \approx 0.18\delta$ and $y \approx 0.43\delta$. (iv) The general distribution of u'/U_0 is shown by the 10% contour, which rises to a peak under the crest and then, in central runs, extends downstream in a band between 0.15δ and 0.3δ. Near the wings, the 10% contour disappears quickly, but the 2% contour extends downstream in the y/δ region where Tollmien–Schlichting waves have their maximum amplitude. This is consistent with the results of WHK.

More detail regarding the shape of the turbulence front is obtained from experiment 5, where the central plane coincides with run (*c*). Contour diagrams of u'/U_0 at 2% intervals were drawn for (T, z)-planes at 9 values of y/δ from 0.05 to 2.0. A contour map of the 2% front of the spot, shown in figure 7(i), was drawn, using the front contours from the diagrams. In the map, the contours for 0.05δ and 0.1δ are closely similar, and deeply reentrant on the centreplane. At 0.2δ the front is slightly convex, and the convexity increases progressively at 0.3δ, 0.4δ and 0.5δ. The turbulence nose (represented by a circle) lies at 0.64δ and $T = 8.2$. At $y = \delta$ the front is again slightly reentrant, and at 1.5δ strongly so.

The recess of the 2% turbulence front at $y \geqslant \delta$ is thought to result from the negative pulses of $\bar{V}$, shown in figure 5 for experiment 1, and in figure 7(ii) for runs (*b*), (*c*) and (*d*) of experiment 5. The continuous lines in 7(ii) are the front contours of u'/U_0 at 2% intervals, and the dashed lines are all the negative contours of $\bar{V}/U_0$ at 1% intervals. $\bar{V}$ is more intense and more deeply penetrating in run (*c*) on the centreplane than in adjacent runs. The *laminar* V-pulses appear to be drawn to the low-pressure

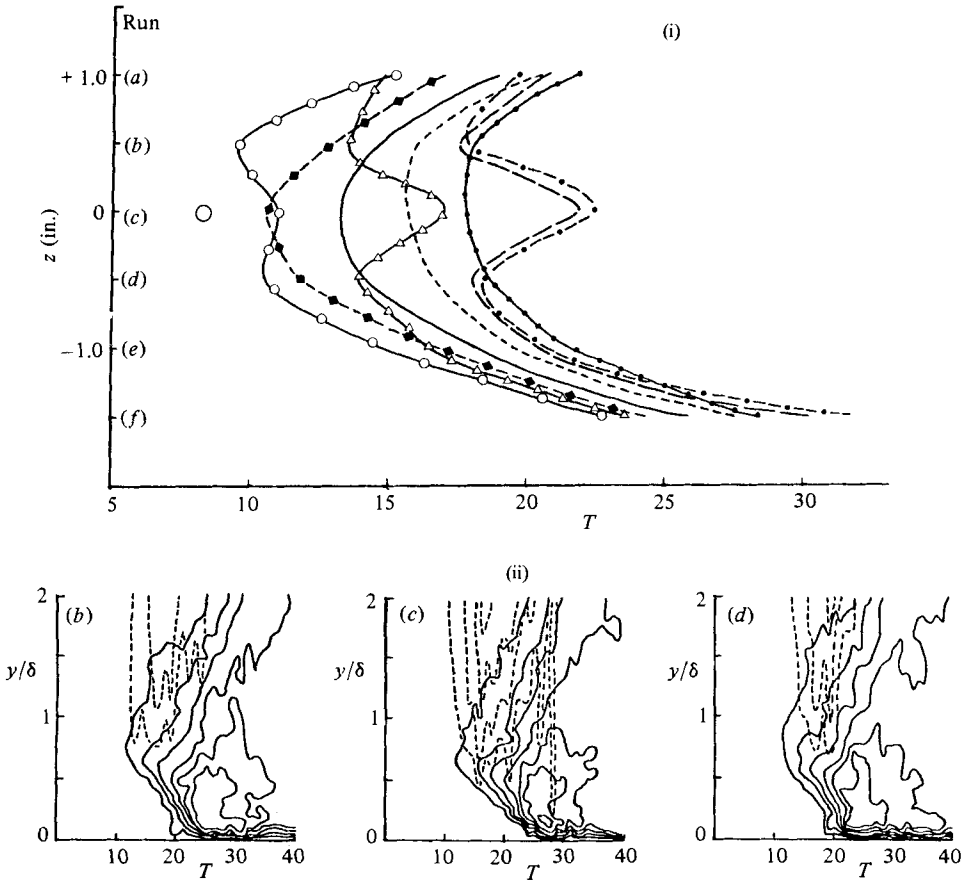

FIGURE 7i, ii. For caption see facing page.

region at the front of the spot. It may also be noted here that the general level of turbulence in experiment 5 is about 2 % lower than in experiment 1. This difference may be partly accounted for by the effect of higher U_0 on our process of spot excitation, but at constant U_0 the turbulence intensity decreases with distance from the source.

The recess near the plate in figure 7 (i) must result from the encounter between the Blasius flow and the rapidly advancing turbulence front. The u'/U_0 intensities near this front were examined in the contour diagrams for the different (T, z)-planes. At 0.05δ the front contours were irregular, rising to 10 % in 4 T-units; at 0.1δ they were more irregular, rising to 16 % in 4.5 T-units. At 0.2δ there was no irregularity; the contours between 2 and 12 % were equally spaced, and for the 3 central runs were nearly parallel to the z-axis, with a constant gradient $\Delta(u'/U_0)/\Delta T$ of 0.44. Thereafter u'/U_0 fell to around 10 % for the rest of the recording. The constant gradient at the front persisted until y exceeded 0.4δ, after which the gradient decreased more rapidly. From these observations it appears that the high rate of turbulence creation occurs within 0.2δ of the plate surface.

The high-turbulence region close to the plate is not recorded in our figure 4. It is possible that the turbulence frequencies involved in experiment 1 exceeded our upper limit of detection of 750 Hz.

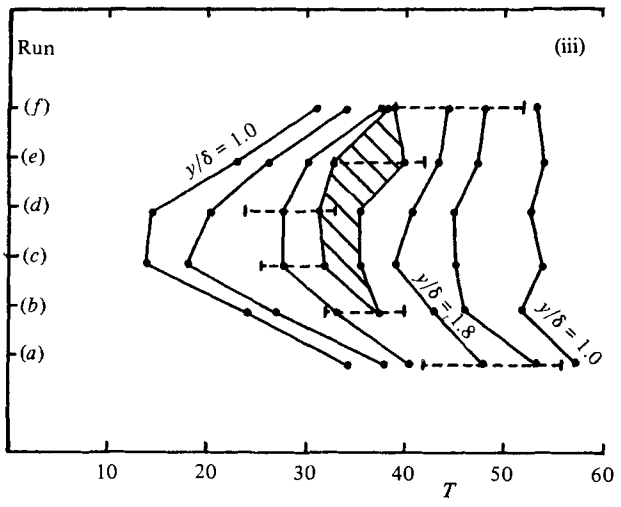

FIGURE 7. (i) Contour map of the turbulence front in experiment 5. Projections on the (T, z)-plane of $u'/U_0 = 0.02$ at various constant values of y/δ. $U_0 = 43.5$ ft/s (13.26 m/s), $x = 4.420$ ft (1.347 m). The nose of u'/U_0 at $y/\delta = 0.64$ is indicated by a circle. ●--●, $y/\delta = 0.05$; ---, 0.1; ●——●, 0.2; ---, 0.3; ——, 0.4; ◆--◆, 0.5; ○——○, 1.0; △——△, 1.5. (ii) Superposition of all negative contours of constant $\overline{V}/U_0$ on contours of constant u'/U_0 for runs (*b*)–(*d*) of experiment 5. $U_0 = 43.5$ ft/s (13.26 m/s), $x = 4.420$ ft (1.347 m). Run (*c*) coincides with the plane of symmetry. ——, contours of u'/U_0 at 2% intervals; – – – –, contours of $-\overline{V}/U_0$ at 1% intervals; zero contours omitted. (iii) Contour map of the crest of the spot in experiment 1. $U_0 = 28.5$ ft/s (8.69 m/s), $x = 2.427$ ft (74 cm). Projection on the (T, z)-plane of the 95% contours of $\overline{U}/U_0$ for y/δ values 1.0, 1.4 and 1.8 and 2.2. The dashed lines parallel to the T-axis are the projections of 14% contours of u'/U_0 enclosing the maximum-turbulence region.

Figure 6(ii) shows the most interesting part of the spanwise flow, $\overline{W}/U_0$, the contours being drawn at 4% intervals with zero contours indicated. Between the plate and $y = 0.2\delta$, the values are predominantly negative on both sides of the centreplane (i.e. antisymmetric). $-\overline{W}/U_0$ is markedly variable in the x-direction, and occasionally exceeds 12%. Between 0.2 and 0.35δ, the values are positive on both sides of the centreplane, and usually remain below 4%. Above 0.35δ the field of flow becomes on the whole symmetric, and directed mainly away from the centreplane. Values of $|\overline{W}|/U_0$ above 0.04 in this region occur infrequently and have an apparently random distribution. In the region of the nose, $\overline{W}/U_0$ is symmetric, directed towards the centreplane above the nose, and away from it below the nose.

The antisymmetric behaviour of the sublayer is evident also in figure 5, which shows strong bursts of positive $\overline{V}/U_0$ arising in the sublayer at intervals of about $10T$. These bursts occur alternately on opposite sides of the centreplane in figures 5(*c*) and (*d*). In experiment 2, similar strong positive $\overline{V}$-pulses appear at intervals of about $15T$. They also occur alternately in runs (*b*) and (*d*) on opposite sides of the centreplane. In experiment 5 the positive $\overline{V}$ was relatively weak on the centreplane, but on each side of that plane, a pattern of positive pulses appeared at intervals of about $23T$. Such pulses contribute to the formation of the large eddies at the crest of the spot which show related periodicities.

Hydrogen-bubble photographs of the flow in turbulent spots have been published by Matsui (1980). Plan views of the flow at low levels are seen in takes 3–6 of figure 4 in that paper. These show that hairpin vortices, which could be associated with bursts, occur alternately on opposite sides of the centreplane.

4. Energy thickness in the spot

4.1. *Evaluation of* δ_3, ${}_s\delta_3$ *and* $\Delta\delta_3$

The turbulent spot – like the Blasius boundary layer – grows by extracting energy from the free stream in which it is formed, and the energy thickness is given by

$$\delta_3 = \int_0^\infty \frac{U}{U_0}\left[1-\left(\frac{U}{U_0}\right)^2\right]\mathrm{d}y.$$

An appropriate value of δ_3 at a chosen time T during the passage of a spot over the probe can be found from measured values of $\overline{U}/U_0$, like those in figure 3, using the mean value of $\overline{U}/U_0$ in each contour interval with $\mathrm{d}y$ as the distance between the two contours at time T. The limits of integration may be taken, without serious distortion of the results, as the values of y at which $\overline{U} = 0$ and $\overline{U} = 0.95U_0$. Such calculations have been made for experiments 1 and 2, at intervals of $2.5T$-units. The results are shown as log δ_3 versus T in figures 8 and 9. In experiment 2 the values of δ_3 over the crest are incomplete.

To examine the flow in the sublayer, the part of the integral between the contours $\overline{U} = 0$ and $\overline{U} = 0.45U_0$ was noted. The values, denoted by ${}_s\delta_3$, are shown on the graphs. For Blasius flow $\delta_3 = 0.70$ (computed to $0.95U_0$) and ${}_s\delta_3 = 0.20$.

Each evaluation of δ_3 was found as the sum of 19 partial (i.e. local) values, $\Delta\delta_3$. By noting the mean y-position of each partial value, the distribution of large values of $\Delta\delta_3$ in any complete run could be examined. A typical map of the large $\Delta\delta_3$ values is shown in figure 10 for run (*d*) in experiment 1. Values of $\Delta\delta_3$ above 0.15 are marked on the map with filled circles of four sizes, representing four groups of $\Delta\delta_3$ with lower limits respectively of 0.15, 0.2, 0.25 and 0.3. The figure also shows the 95 % contour of $\overline{U}/U_0$, the 2 % contour of u'/U_0 and the region of maximum observed turbulence. Near the plane of symmetry in experiment 1, values of $\Delta\delta_3$ greater than 0.25 occurred *randomly* at a few points in the region $y > 1.2\delta$, and *more frequently* in the region $0.6 < y/\delta \leqslant 1.2$. Below $y = 0.6\delta$ large values of $\Delta\delta_3$ occurred only in the band $0.3 < y/\delta < 0.45$, and there they occurred *systematically* in every integral calculation in the interval $30 \leqslant T \leqslant 60$, which became $50 \leqslant T \leqslant 62.5$ in run (*a*).

4.2. *Spot structure*

In figures 8 and 9 the graph of δ_3 lies entirely above the Blasius value until $T = 57.5$ in figure 8 and $T = 90$ in figure 9. After these times δ_3 falls below 0.70. By contrast, apart from a few high points near the turbulence front, the ${}_s\delta_3$ points lie entirely below the Blasius value 0.20. The graph of ${}_s\delta_3$ falls rather irregularly until $T = 57.5$ in figure 8 and $T = 90$ in figure 9; the graph then changes its direction abruptly, and becomes relatively smooth. The abruptness of the change in direction of the ${}_s\delta_3$ graphs, and the agreement in time of that change with a δ_3 condition, shows that a new regime has suddenly been established allowing the sublayer and the higher part of the flow to become directly coupled, and to begin the reconstitution of the laminar boundary-layer flow. The critical point appears to be the point identified as E by CCD.

If before the critical times the two parts of the flow are to be regarded as decoupled, it is necessary to consider what the term 'decoupled' means in this connection. It does not mean that there is any breakdown of the conservation laws of fluid dynamics. It merely means that the two parts of the flow are controlled by different processes. High turbulence in the upper part of the spot consolidates the fluid there, enabling this part to move as a whole (maintaining a speed at its lower boundary much higher

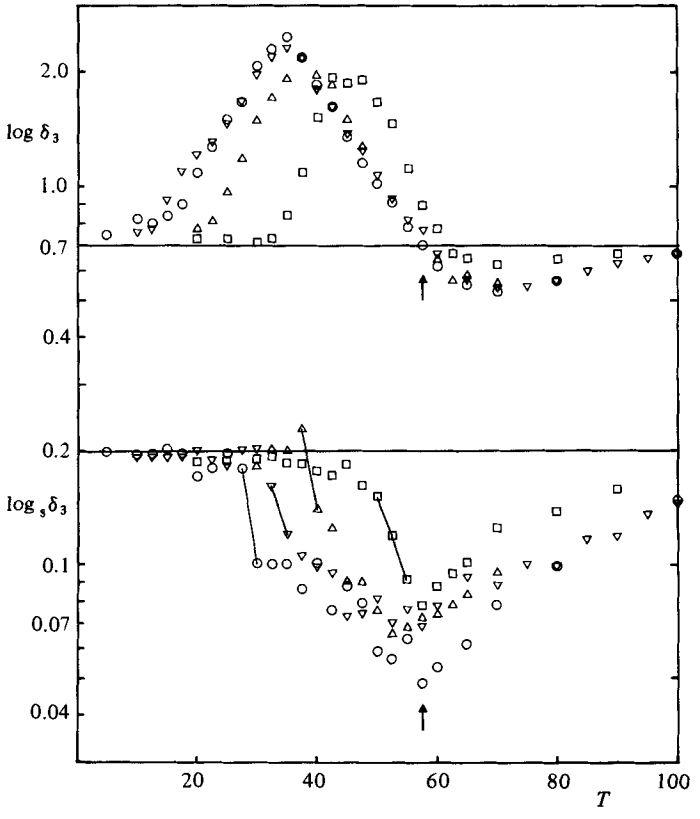

FIGURE 8. Log δ_3 and log $_s\delta_3$ versus T for four runs of experiment 1. $U_0 = 28.5$ ft/s (8.69 m/s), $x = 2.427$ ft (74 cm). □ (*a*); △ (*b*); ▽ (*c*); ○ (*d*). Arrows indicate the conditions permitting reconstitution of the boundary layer. Lines joining adjacent points indicate the beginning of decoupling for each run. The centreplane lies nearer run (*d*) than run (*c*).

than the Blasius speed at the same level), while enabling it also to develop gradually with time. Beneath the high-turbulence region there lies the sublayer with its anomalously high gradient $\partial\overline{U}/\partial y$. Within the sublayer there are thought to be relatively large, low-turbulence eddies acting like ball-bearings or roller-bearings, minimizing the viscous losses. Some evidence for the presence of these eddies in the sublayer is provided by ACSA, and by the large fluctuations of u'/U_0 in figure 4 and those of $_s\delta_3$ in figures 8 and 9. The main control on the sublayer flow is, of course, exercised by the flat plate.

The 'upper part' of the spot includes all the sites of high turbulence creation – including the low-level part at the front of the spot. The interface between the two parts near the front lies where the nearly laminar (high-vorticity) flow in the sublayer is incorporated in the turbulence. Another important source of turbulence is the layer of *systematic* high values of $\Delta\delta_3$, between 0.3δ and 0.45δ, and the band of high turbulence below that layer forms the lower interface.†

The shape of the band of strongly coordinated turbulence seen in the (T, z)-planes of experiment 5 at levels from 0.2δ to over 0.4δ at the front of the spot appears to be the same as the shape of the spot found at low levels by Schubauer & Klebanoff (1956).

† This band of turbulence is thought to be the main source of the trailing vortices, which are a conspicuous feature in photographs of the spots, but are not seen in those taken at very low levels by Matsui (1980).

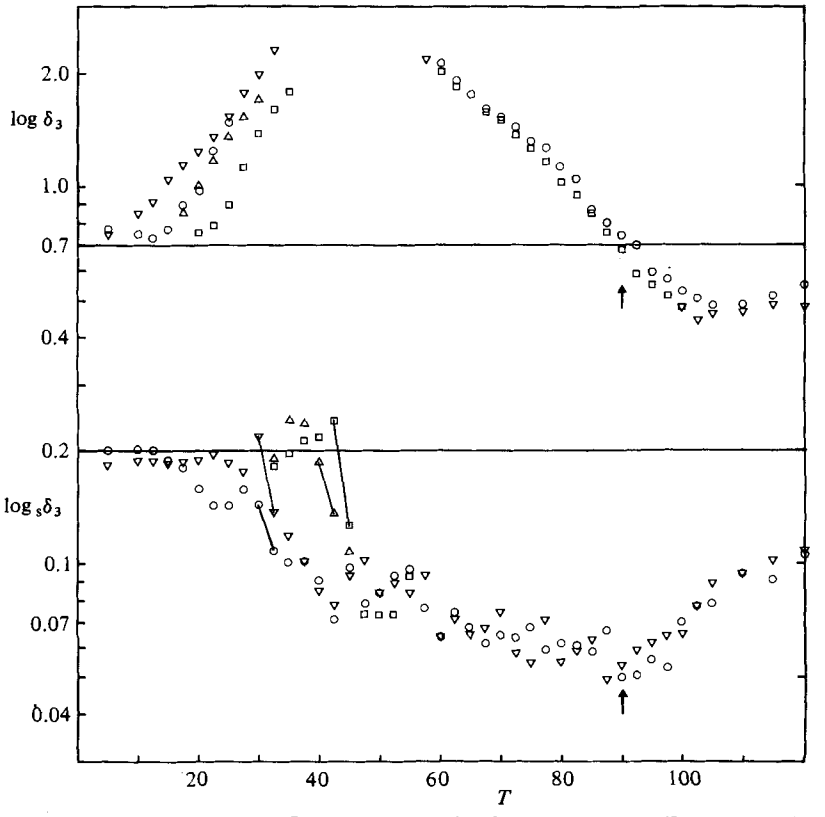

FIGURE 9. Log δ_3 and log $_s\delta_3$ versus T for runs (*c*)–(*f*) of experiment 2. $U_0 = 28.5$ ft/s (8.69 m/s), $x = 3.430$ ft (1.045 m). ○ (*c*); ▽ (*d*); △ (*e*); □ (*f*). Missing points have been omitted to simplify the graph. The centreplane coincides with run (*c*). Otherwise as for figure 8.

In our experiment 5 this band remains parallel to the z-axis for 1.5 in. (3.8 cm), and then bends quite quickly to follow the established shape (see also figure 7iii). The band is thought to be stable enough to exert a strong influence on the fluid in the main body of the spot. If it is continously fed with new fluid – as seems likely – it must be releasing fast-moving fluid into the body of the spot.

In conclusion, we regard the spot as consisting of two parts. The upper part moves forward at relatively high speed over a more passive lower layer. The latter is accelerated at its upper surface until, near the trailing end of the spot, the value of δ_3 there falls to the Blasius value. The Blasius distribution is then slowly re-established. It would be interesting to test whether the thickness of the sublayer is such as to minimize the total rate of energy loss when the turbulent spot is in action. To study the sublayer flow more completely, special methods will be necessary, such as those developed by Offen & Kline (1974).

5. Entrainment

Entrainment has been considered at length by CCD, who gave numerical estimates of the rates of increase of different areas on the central plane of the spots. WZH have also dealt in detail with the subject. In both cases the approach has been through calculations of streamlines and particle paths, and these involve approximate

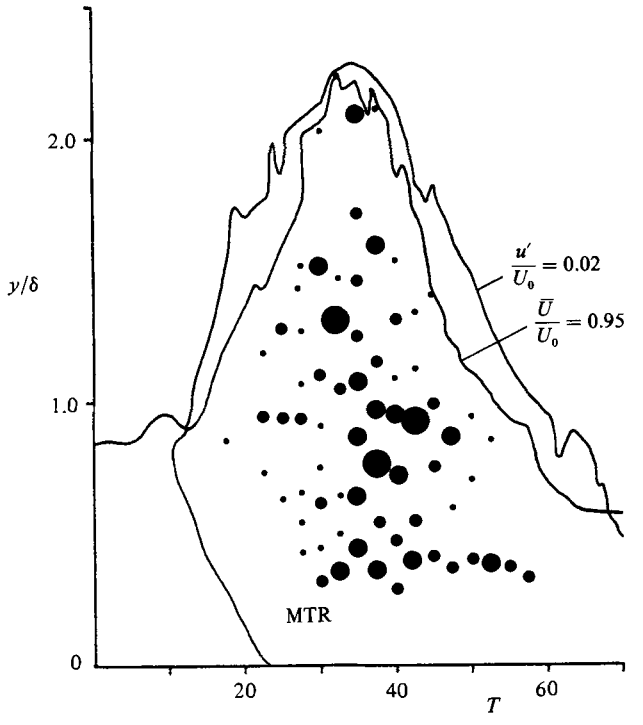

FIGURE 10. Map showing the position in the (T, y)-plane of high values of $\Delta\delta_3$ for run (d) of experiment 1. $U_0 = 28.5$ ft/s (8.69 m/s), $x = 2.427$ ft (74 cm). The solid circles of 4 sizes represent values of $\Delta\delta_3$ classified in 4 groups according to size, the threshold values for these groups being 0.15, 0.2, 0.25 and 0.3.

transformations of recorded $U(t)$ to $U(x)$. CCD point out that it is desirable to consider the physical processes that lead to entrainment, and this we now attempt.

The first step is to define the surface of the spot near the centreplane. Starting from the front of the spot, this surface must begin at the plate, rise through the Blasius layer for $y \leqslant \delta$, and then rise through the free stream to a level above the crest. Beyond the crest, it must pass down through the free stream and then through the calmed region where $\overline{U}/U_0$ is a measured flow. Some parts of this surface can be treated fairly simply.

(i) *The front with* $y > \delta$. Here we can define the front as the surface separating $\partial U/\partial x = 0$ from $\partial U/\partial x \neq 0$. Just inside this surface, $\partial U/\partial x$ is positive, and we have a continuity problem. $\partial V/\partial y + \partial W/\partial z$ must be negative. We know from observation that V is negative there. The main reason for the V-flow is the continuity requirement. The true front of the spot must lie ahead of the first observed negative V, and the V-flow must come from the crest. There should be no entrainment through this front.

(ii) *The rear in the free-stream region.* We can define the front again as the surface separating $\partial U/\partial x = 0$ and $\partial U/\partial x \neq 0$. Just inside the surface, $\partial U/\partial x$ is negative, and the free stream is approaching. There is no continuity problem, but the convection term $U\partial U/\partial x$ is negative, providing an upstream acceleration for the turbulent fluid. The contours in figure 3 show that upstream convection is strong throughout the rear of the spot. All three convection terms in the x-component equation of motion are involved.

(iii) *The front with* $y \leqslant \delta$. Under the nose, figure 6(i) shows (a) that $\overline{U} > U_B$ up

Observed		Calculated %	Observed	Calculated
$\frac{u'}{U_0}$	$\frac{\bar{U}}{U_0}$	$\frac{\bar{U}_c - \bar{U}}{\bar{U}}$	$\frac{u'}{\bar{U}}$	$\frac{u'}{\bar{U}_c}$
0.14	0.40	−1.6 to −4.7	0.350	0.365 to 0.390
0.14	0.45	−1.2 to −3.7	0.311	0.321 to 0.338
0.18	0.40	−2.7 to −7.8	0.450	0.483 to 0.547
0.18	0.45	−2.1 to −6.1	0.400	0.425 to 0.467

TABLE 2. Correction of errors in observed values of $\bar{U}$ and $u'/\bar{U}$

to 0.7δ, where $U_B = 0.9U_0$, and (*b*) that $\partial U/\partial x$ is still positive. Entrainment should not occur. High turbulence is, however, observed below 0.2δ, and C_p at the plate is depressed. We suggest that the resulting disturbance of the previously laminar, high-vorticity, Blasius flow close to the plate causes its vorticity to become turbulent. The turbulence front is known to advance at $\sim 0.88U_0$, while hot-wire measurements of the local velocity in the fluid give much smaller speeds. Entrainment is therefore confined to very low levels, and is operated by direct transition to turbulence. Figure 4 shows that the turbulence gradient normal to the plate rises rapidly behind the front. The entrainment volume is large, considering the area of the entry 'window'. Convection of turbulence in the normal direction will be operated by $U\partial V/\partial x + V\partial V/\partial y$. Figure 5(*d*) shows that near the centreplane there are positive contours of V lying between negative pulses, and there $U\partial V/\partial x$ is alternating in sign while $V\partial V/\partial y$ is positive. Calculation of entrainment at the low levels is complicated by the reentrant shape of the front in the centreplane. As $|z|$ increases, the front becomes convex, and entrainment may be reduced by spanwise flow leading to rolling-up of the laminar vorticity close to the plate, and to spanwise growth of the spot.

(iv) *The crest of the spot.* This is clearly the most difficult part of the boundary to deal with. The 'signature' of $(U - U_B)/U_0$ shown in figure 1 of Van Atta *et al.* (1982) might prove useful, since the graph for $y = 3.18$ cm shows only the effects of positive and negative variations of V, and no short-time variations associated with the large eddies.

This work was supported in its early stages by the award to J. Barrow of a grant from the Ministry of Defence.

Appendix. Estimates of errors of measurement in figures 3 and 4

The results in figures 3 and 4 are not corrected for the errors of observation arising when hot-wire voltages are measured in a turbulent field and converted to velocities by King's law. The highest observed values of u'/U_0 lie in the range 14–18 %, and occur close to the 40 and 45 % contours of $\bar{U}/U_0$, in a region where v'/u' is considered to reach between 0.8 and 1.0. Using these values in equations (8) and (9N) of Klatt (1973) leads to the estimates of $(\bar{U}_c - \bar{U})/\bar{U}$ % and $(u'/\bar{U})_c$ shown in table 2, where suffix c indicates corrected values.

An estimate of the maximum error in $u'/\bar{U}$ could also be made directly in the region of maximum turbulence from the observation that, in a small number of the sets of 80 measurements of U made in this region, one (and very occasionally two) of the 80

measurements fell to about zero. Assuming that the distribution of U is approximately Gaussian, the local value of $u'/\overline{U}$ in such cases must be about 0.5. This is consistent with the results in table 2.

REFERENCES

ANTONIA, R. A., CHAMBERS, A. J., SOKOLOV, M. & VAN ATTA, C. W. 1981 *J. Fluid Mech.* **108**, 317.

BARROW, J. 1975 Ph.D. thesis, University of Edinburgh.

CANTWELL, B., COLES, D. & DIMOTAKIS, P. 1978 *J. Fluid Mech.* **87**, 641.

COLES, D. & BARKER, S. J. 1975 Some remarks on a synthetic turbulent boundary layer. In *Turbulent Mixing in Nonreactive and Reactive Flows* (ed. S. N. B. Murthy), p. 285. Plenum.

ELDER, J. W. 1960 *J. Fluid Mech.* **9**, 235.

EMMONS, H. W. 1951 *J. Aero. Sci.* **18**, 490.

KLATT, F. 1973 *Disa Info.* no. 14, p. 25.

MATSUI, T. 1980 In *Laminar–Turbulent Transition* (ed. R. Eppler & H. Fasel), p. 288. Springer.

MAUTNER, T. S. & VAN ATTA, C. W. 1982 *J. Fluid Mech.* **118**, 59.

OFFEN, G. R. & KLINE, S. J. 1974 *J. Fluid Mech.* **62**, 223.

ROBERTSON, T. & BURNS, J. G. 1972 *J. Phys.* E: *Sci. Instrum.* **5**, 598.

SCHUBAUER, G. B. & KLEBANOFF, P. S. 1956 *NACA Rep.* 1289.

VAN ATTA, C. W. & HELLAND, K. N. 1980 *J. Fluid Mech.* **100**, 243.

VAN ATTA, C. W., SOKOLOV, M., ANTONIA, R. A. & CHAMBERS, A. J. 1982 *Phys. Fluids* **25**, 424.

WYGNANSKI, I., HARITONIDIS, J. H. & KAPLAN, R. E. 1979 *J. Fluid Mech.* **92**, 505.

WYGNANSKI, I., SOKOLOV, M. & FRIEDMAN, D. 1976 *J. Fluid Mech.* **78**, 785.

WYGNANSKI, I., ZILBERMAN, M. & HARITONIDIS, J. H. 1982 *J. Fluid Mech.* **123**, 69.

ZILBERMAN, M., WYGNANSKI, I. & KAPLAN, R. E. 1977 *Phys. Fluids Suppl.* **20**, S258.